COMPUTER METHODS IN MATERIALS SCIENCE

2021, vol. 21, no. 2, 83–94
https://doi.org/10.7494/cmms.2021.2.0744

Artificial intelligence approach for detecting material deterioration in hybrid building constructions

Andrei V. Chesnokov*, Vitalii V. Mikhailov, Ivan V. Dolmatov

The Faculty of Civil Engineering, Lipetsk State Technical University, Moskovskaya street 30, 398600 Lipetsk, Russian Federation.

Abstract

Hybrid constructions include heterogeneous materials with different behaviors under load. The aim is to achieve a so-called synergistic effect when the advantages of particular structural elements complement each other in a unified system.

The building constructions considered in the research include high-strength steel cables, fiberglass rods, and flexible polymer membranes. The membrane is attached to the rods which have been elastically bent from the initially straight shape into an arch-like form.

Structural materials inevitably deteriorate during a long operational period. The present study focuses on detecting material deterioration using Artificial Neural Networks (ANNs), which belong to the scope of intelligent techniques for data analysis. Appropriate ANN structures and required features are proposed. A semi-supervised learning strategy is used. The approach allows the training of the networks with normal data only derived from the construction without defects. Material degradation is detected by the level of reconstruction error produced by the network given the input data.

The work contributes to the field of structural health monitoring of hybrid building constructions. It provides the opportunity to detect material deterioration given the forces in particular structural elements.

Keywords: hybrid constructions, material deterioration, artificial neural network, semi-supervised machine learning

1. Introduction

Hybrid building constructions consist of heterogeneous materials which behave differently under external load. Along with ordinary structural steel, they include high-strength cables, fiberglass rods, and flexible polymer membranes. The aim is to achieve a so-called synergistic effect when advantages of particular structural elements complement each other in the unified system, and every structural member behaves in the most efficient way.

The scope of hybrid constructions encompasses the roofs and facades of permanent buildings, as well as temporary canopies for exhibitions, recreation areas, points of retail, and construction sites.

Structural materials inevitably deteriorate during their operational period. The deterioration results in aesthetic, functional, and technical defects (Sommerville, 2007; Wang et al., 2015). The first type of defects results in poor visual performance of the building. Functional defects reduce structural serviceability and bring about the growth of expenditures. The last type of defects diminishes the load-bearing capacity of structural elements. It results in decreasing the reliability of the whole construction.

Technical defects affect the ultimate limit state of the hybrid buildings. They include the degradation of fiberglass polymer, creep of the membrane and the cables,

* Corresponding author: andreychess742@gmail.com
ORCID ID's: 0000-0003-3687-0510 (A.V. Chesnokov), 0000-0001-8274-9346 (V.V. Mikhailov), 0000-0002-7066-3366 (I.V. Dolmatov)

as well as the emergence of tiny slits or tearing in the membrane surface. The slits are accidental and initially hidden from view (Gipperich et al., 2004). They, however, result in stress concentration and tend to quickly propagate throughout the whole membrane surface.

Fiberglass polymers lose their strength and become brittle. Initial E-modulus gradually alters with time. It should be taken into account in the design stage of hybrid constructions which are intended for long-term use in permanent buildings.

Creep of the membrane and the cables results in the elongation of structural members and stress relaxation. The flexible elements of the construction which need to retain tension under external loads may slack due to creep, and the structure becomes out-of-order.

Creep also gives rise to rainwater ponding and excessive movement of the under-stressed membrane. The ponding starts a so-called 'chain reaction' of increasing local loads until the structural collapse. Excessive movement or 'flapping' entails noise generation and stimulates fatigue wear and tear of the membrane (Bridgens et al., 2004).

The present study focuses on the detection of material deterioration using Artificial Neural Networks (ANNs), which belong to the scope of intelligent techniques for data analysis. A construction without any defects is considered 'normal' while a deteriorated one is called 'anomalous'. The task for the ANN is to provide results for distinguishing between these classes.

ANNs consist of a number of nodes interconnected with links. The nodes, like biological neurons, non-linear transform the input signal into the output one. A link, or a synapse, transmits the signal between two neurons using an appropriate weight coefficient simulating 'agitation and inhibition' in a biological nervous system.

Having adjusted the weight coefficients, the ANN is able to process fuzzy data in solving complex problems for which appropriate mathematical models have not been developed.

ANNs are used for structural health monitoring (Pozo et al., 2017) and material behavior simulation (Colasante & Gosling, 2016). They are successfully applied in the field of anomaly detection. ANNs are an appropriate tool for separating deteriorated constructions from normal ones.

Supervised, unsupervised, and semi-supervised approaches are used for detecting anomalies by the ANNs (Chandola et al., 2009).

An unsupervised approach needs no labeled data but requires the anomalous cases to be rare. Frequent anomalies are misclassified as normal. In addition, the unsupervised detection system having no given data with 'right answers' results in a high false alarm rate.

A supervised machine learning strategy requires labeled instances for all the deterioration cases to be provided. This approach, however, suffers from a huge manifold of eventual anomalous scenarios, which are hard to be taken into account in the design stage.

A semi-supervised approach (Hodge & Austin, 2004), in contrast to the supervised one, only requires normal cases. Normal data are derived from the construction without defects. Material degradation is detected by the level of reconstruction error produced by the trained model given the input data.

2. The hybrid building constructions

The hybrid construction considered in the research belongs to bending-active structures which are shaped into arch-like forms by means of elastic deformation of their primary bearer rods (Lienhard et al., 2013; Van Mele et al., 2013).

The construction consists of a framework and a flexible membrane shell (Fig. 1) (Chesnokov et al., 2017, 2019). The bottom chord of the framework includes steel cables and hinged spreaders. The spreaders are of ordinary structural steel with Young's modulus E_s = 260 GPa and flexural strength R_s = 240 MPa. The cables are composed of high-strength wire ropes with E_{cab} = 130 GPa and R_{cab} = 700 MPa.

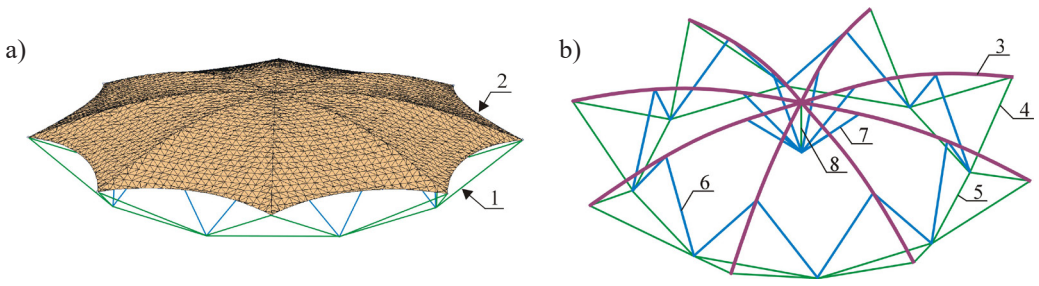

Fig. 1. The hybrid construction: a) axonometric view; b) bearer framework; 1 – bottom chord; 2 – flexible membrane shell; 3 – fiberglass rod; 4 – diagonal cable; 5 – hoop cable; 6, 7 – spreaders; 8 – tie

The top chord is made of fiberglass rods with initial Young's modulus E_{fb} = 24 GPa and the strength R_{fb} = 185 MPa. The rods are bent from the initially straight shape into arch-like form by means of pre-stressing of the steel cables. The initial span of the frame, equal to 12 m, is reduced by 0.35 m, while the top chord camber rises up to 1.15 m.

The membrane which belongs to architectural fabrics is attached to the fiberglass rods. It is an inherent part of the construction for providing the cladding and preventing buckling of the rods. The membrane consists of flexible threads and a polymer coating. Its warp-to-weft stiffness is 1200 × 800 kN/m.

3. Method

3.1. External loads simulation

External loads are applied in the Z-direction (Fig. 2). Nonuniform impacts are simulated by the reduction factor k_r, $k_r \in [0, ..., 1]$:

$$Q_r = k_f \cdot Q_f \tag{1}$$

where Q_f and Q_r are full and reduced loads [kN/m^2].

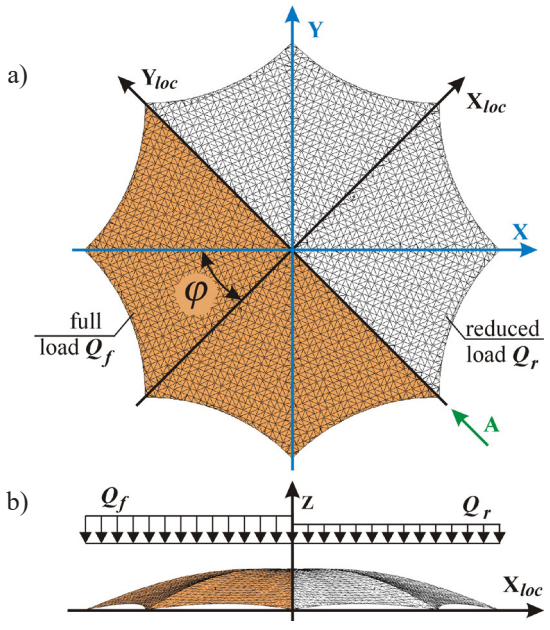

Fig. 2. External loads: a) plan view of the load zones; b) view along the line A

An external load is associated with a local coordinate system (X_{loc}, Y_{loc}, Z) that rotates about the global Z-axis by an angle φ. Each position of the local coordinate system (X_{loc}, Y_{loc}, Z) simulates non-uniform impact centered on a particular rib of the construction.

3.2. Simulation of the material deterioration

The following deterioration scenarios are considered (Fig. 3):

- ageing of the fiberglass rods (all the elements and a single one);
- slackening of the catenary cables (all the catenaries and the ones which belong to a quarter of the surface);
- slackening of the polymer membrane (the whole surface and a quarter of it);
- membrane tearing.

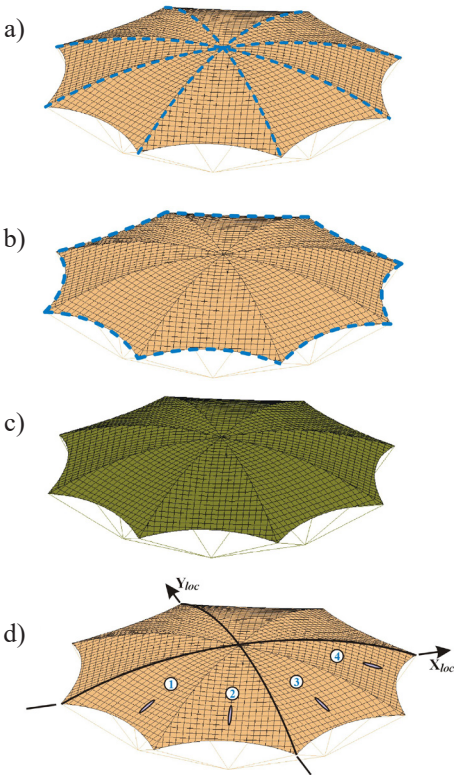

Fig. 3. Material deterioration considered: a) ageing of fiberglass rods; b) slackening of the catenary cables; c) slackening of the polymer membrane; d) membrane tearing (local slits in sectors 1–4 of the surface)

Static analysis of the constructions is performed in the software EASY-2020 using the non-linear Finite Element technique.

The ageing of fiberglass rods is introduced into the structural model by using long-term E-modulus instead of short-term values. Cable and membrane slackening due to creep is taken into account by means of multiplying the initial element lengths by the factor:

$$k_{\varepsilon_c} = 1 + \varepsilon_c \tag{2}$$

where ε_c is the creep relative elongation: ε_c = 0.6% for the polymer membrane and ε_c = 0.05% for the steel cables.

The polymer membrane is simulated in the EASY-2020 software by a number of links forming a mesh-like surface. The surface with particular links removed is a model of the membrane tearing adopted in the present study.

Membrane tearing in any sector, denoted in Fig. 3d, is considered. Sector numbers are indicated in the local coordinate system (X_{loc}, Y_{loc}, Z), which is associated with load zones (Fig. 2): the first sector is situated in the fully loaded area of the membrane, while the last sector is in the center of the reduced load.

3.3. The feature selection

A finite-element simulation of the hybrid constructions in EASY-2020 software shows the influence of material deterioration on the structural behavior of the frame. In-plane bending moments M_v in the fiberglass rods of the top chord (moments in the vertical plane) are susceptible to ageing of the material and slackening of structural elements, while tearing of the membrane brings about out-plane moment variation M_w (moments in the horizontal plane), Figures 4 and 5.

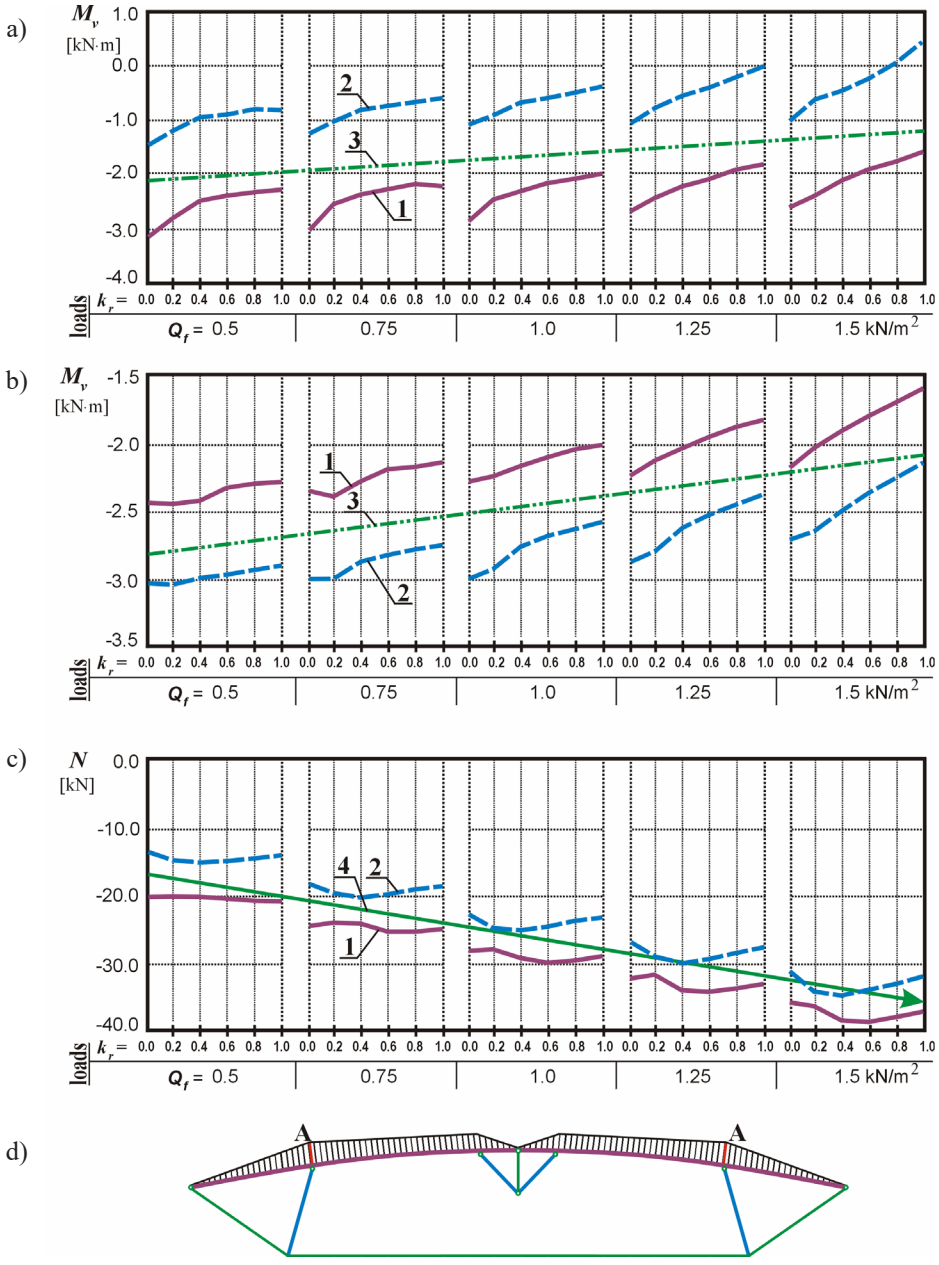

Fig. 4. Graphs of in-plane bending moments M_v and axial forces N in the top chord of the construction given the deterioration scenario: a) ageing of fiberglass rods (minimum moments in nodes A of all the ribs); b) polymer membrane slackening on the whole surface (maximum moments in nodes A); c) typical graphs of minimum axial forces N in the fiberglass rods; d) cross section view of the structural frame (nodes A and M_v diagrams are shown); 1 – reference state (no material deterioration); 2 – deteriorated state; 3 – separation line; 4 – trend line

In the case of the ageing of the fiberglass rods, both maximum and minimum values of bending moments M_v can be linearly separated from the reference state. For cable and membrane slackening cases, either maximum or minimum M_v-values are linearly separable. Thus, extreme values of in-plane bending moments M_v allow detecting material deterioration in the construction given the external load Q_f. The magnitude of Q_f is defined by the axial force N in the top chord because N-graphs are close to the trend line (Fig. 4c).

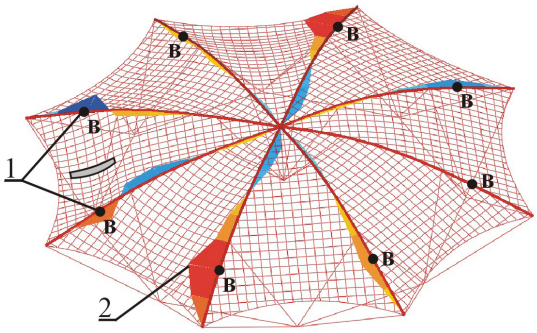

Fig. 5. Diagrams of out-of-plane bending moments M_w in the fiberglass rods of the top chord: 1 – moments brought about by the slit; 2 – load-induced moments

Membrane damage (tearing or slit) causes triangular-like moments M_w in the horizontal plane (Fig. 5). Non-uniform external loads also result in M_w-diagrams which may be confused with tearing-induced moments. In order to detect the membrane damage, the moments M_w are taken in all the fiberglass rods (nodes B, marked in Fig. 5). It allows to reliably separate the case of the membrane tearing from complexly loaded but not deteriorated construction.

3.4. Semi-supervised machine learning for detecting material deterioration

The approach used in the present study for detecting material deterioration includes developing machine learning models in the form of artificial neural networks (ANNs). The ANN provides the resultant vector $\vec{Y} = (y_1, ..., y_i, ..., y_{N_0})^T$ given the input data-vector $\vec{X} = (x_1, ..., x_i, ..., x_{N_0})^T$ (Fig. 6). The vector $\vec{X}$ contains structural parameters x_i (features) which are susceptible to the influence of possible deterioration cases. In the present study, axial forces and bending moments in the fiberglass rods of the top chord of the construction are included in the $\vec{X}$-vectors.

Fig. 6. Schematic diagram of the ANN

The hybrid construction is classified using condition (3) as follows: if the discrepancy δ_{max} (4) exceeds the threshold Δ_{max} (5) the construction is considered damaged, otherwise, it is classified as normal.

$$\delta_{max} > \Delta_{max} \tag{3}$$

The discrepancy for a particular hybrid construction (a sample) is obtained as follows:

$$\delta_{max} = \max(|y_i - x_i|) \tag{4}$$

where x_i and y_i are the components of $\vec{X}$ and $\vec{Y}$ vectors, $i \in [1, ..., N_0]$.

The threshold Δ_{max} is the maximum discrepancy achieved by the trained ANN over all the samples taken from the training dataset $\vec{\Omega}_{tr} = (\vec{X}_1, ..., \vec{X}_{n_{tr}})^T$:

$$\Delta_{max} = \max(\delta_{max,t}) \tag{5}$$

where: t – the number of a training sample, $t \in [1, ..., n_{tr}]$; n_{tr} – the size of the training dataset.

Estimation of the overall quality of the considered classification approach is performed using testing $\vec{\Omega}_{test} = (\vec{X}_1, ..., \vec{X}_{n_{test}})^T$, and operational $\vec{\Omega}_{op} = (\vec{X}_1, ..., \vec{X}_{n_{op}})^T$, datasets after the process of training of the ANN is completed.

The testing dataset $\vec{\Omega}_{test}$, as well as the training one $\vec{\Omega}_{tr}$, are obtained for so called reference state of the construction having no damage of its structural members. The operational dataset $\vec{\Omega}_{op}$ is obtained given particular deterioration or a material degradation case.

The classification is correct in the following cases:

- the condition (3) meets for the operational samples;
- the condition (3) fails for the testing samples.

The proportion of misclassified cases is estimated by the following error metrics:

$$\xi_p = \frac{n_p}{n_{test}} \cdot 100\% \tag{6}$$

$$\xi_n = \frac{n_n}{n_{op}} \cdot 100\% \tag{7}$$

where: ξ_p, ξ_n – false positive and false negative rates [%]; n_p – the number of samples, belonging to the testing dataset $\vec{\Omega}_{test}$, for which the condition (3) satisfies; n_n – the number of samples, belonging to the operational dataset $\vec{\Omega}_{op}$, for which the condition (3) fails; n_{test}, n_{op} – the sizes of the testing and operational datasets, respectively.

The false-positive metric estimates the so-called 'false alarm' rate, when good construction is misclassified as damaged. The false-negative metric estimates the proportion of really deteriorated samples is misclassified as normal.

3.5. Artificial neural networks

Feedforward artificial neural network (ANN) or multilayer perceptron has proven its efficiency in a number of engineering problems (Horr et al., 2003; Kaveh & Dehkordi, 2003). It is adopted in the present study to build the models used for the classification of the hybrid construction into normal or deteriorated classes.

ANN consists of successively arranged layers (Fig. 6). The general structure of the network may be represented as follows: $N_0 - N_1$, ..., $N_h - N_{h+1}$, where N_j is the number of processing units (artificial neurons) belonging to the layer j, $j \in [0, ..., (h + 1)]$, where h is the number of hidden layers in the network.

Each neuron $i_j \in [1, ..., N_j]$ of the layer j performs the following transformation using an activation function f_j (Fig. 7):

$$v_{i_j} = f_j(u_{i_j}) \tag{8}$$

where u_{i_j} and v_{i_j} are the components of the incoming vector $\vec{U}_j$ which is received by the layer, and the resultant vector $\vec{V}_j$ which is generated by the layer, respectively.

Vectors $\vec{V}_j$, except the one which belongs to the output layer of the ANN, are supplemented with the bias term $v_0 = 1.0$ (Fig. 7).

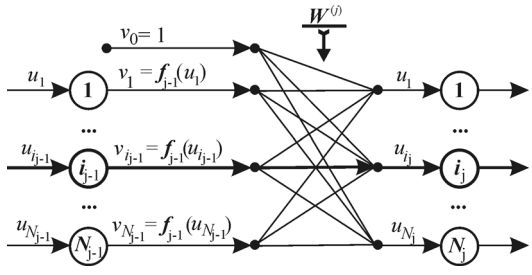

Fig. 7. Data flow between adjacent layers of the ANN

Linear activation function is used for the input and the output layers of the ANN:

$$f_j(u) = u, \text{ if } j = 0 \text{ or } j = h + 1 \tag{9}$$

Sigmoid-type activation function is applied for the hidden layers:

$$f_j(u) = \frac{2}{1 + e^{-\beta \cdot u}} - 1, \text{ if } j \in [1, ..., h] \tag{10}$$

where β-factor is adopted equal to 3.0.

Sigmoid function (10) consists of two distinct domains: quasi-linear central region and, so-called, saturated regions at the ends (Fig. 8). The function, being differentiable, can be used in gradient optimization procedures. The sigmoid function allows the outputs of the hidden layers to be kept in the range [–1, ..., +1], preventing the divergence of the iteration process needed to obtain the parameters of the network.

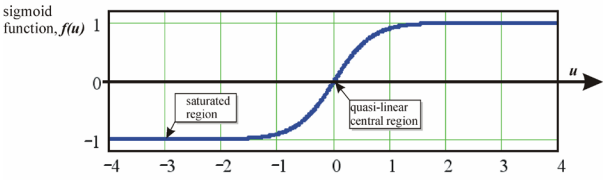

Fig. 8. Sigmoid-type activation function, β = 3.0

The input layer of the ANN ($j = 0$) receives a normalized data-vector $\vec{U}_0 = \vec{X}_{norm}$. Normalization is the mapping of the given $\vec{X}$-vector into the dimensionless range $x_{norm,i} \in [0.0, ..., 1.0]$. The output and the hidden layers ($j \in [1, ..., (h + 1)]$) receive weighted results generated by the previous layers (Fig. 7):

$$\vec{U}_j = [W^{(j)}] \cdot \vec{V}_{j-1} \tag{11}$$

where $W^{(j)}$ is an $[N_j \times (N_{j-1} + 1)]$-matrix of weight factors.

The output layer of the ANN ($j = h + 1$) generates the resultant $\vec{Y}$-vector:

$$\vec{Y} = \vec{V}_{h+1} \tag{12}$$

The matrices $W^{(j)}$ are initialized with random values in the range $[-2, ..., +2] / \sqrt{N_{j-1}}$ (Thimm & Fiesler, 1995). During the training process, they are adjusted by means of the gradient descent optimization technique:

$$w^j_{i_j,k} = w^j_{i_j,k} - \eta_j \cdot \frac{\partial E_t}{\partial w^j_{i_j,k}} \tag{13}$$

where: $w^j i_{j,k}$ – the element of the matrix $W^{(j)}$, $i_j \in [1, ..., N_j]$, $k \in [0, ..., N_{j-1}]$; E_t – the mean squared error (MSE) of a sample; η_j – the learning rate for the layer j (Osovskiy, 2002):

$$\eta_j = \frac{1}{N_{j-1} + 1} \tag{14}$$

The mean squared error for a particular training sample $t \in [1, ..., n_{tr}]$ is obtained as follows:

$$E_t = \frac{1}{N_0}\sum_{i=1}^{N_0}(y_i - x_i)^2 \tag{15}$$

where: x_i – the components of $\vec{X}_t$-vector from the training dataset $\vec{\Omega}_{tr}$; y_i – the components of the resultant vector $\vec{Y}$ given the vector $\vec{X}_t$.

The samples for adjusting the weights (13) are picked from the training dataset $\vec{\Omega}_{tr}$ in random order. When the dataset is exhausted, the total average error is calculated for the current training epoch as follows:

$$E = \frac{1}{n_{tr}}\sum_{t=1}^{n_{tr}} E_t \tag{16}$$

The training process is considered finished when the variation of the error E becomes less than the limit value ζ_{lim}:

$$|\zeta| < \zeta_{\text{lim}} \tag{17}$$

where: ζ_{lim} – adopted equal to 5%; ζ – the variation:

$$\zeta = \frac{E_{e-1} - E_e}{E_e}\cdot 100\% \tag{18}$$

where E_e and E_{e-1} are the errors (16) on the current and on the previous epochs, respectively.

The training is also wrapped if the variation ζ becomes either steadily negative or oscillating.

3.6. The ANN structure

Material deterioration cases considered in the present study form two separate groups which need different feature sets to be detected. The first group includes fiberglass top chord ageing, as well as catenary cables and polymer membrane slackening. The corresponding input vector consists of three features:

$$\vec{X}_I = [N_{\text{min}}, M_{v,\text{max}}, M_{v,\text{min}}]^T \tag{19}$$

Membrane damages compose the second group of material deterioration cases. The feature set needed for achieving appropriate accuracy includes bending moments M_w in all the rods of the top chord. Considering eight ribs in the present study, the input vector is written as follows:

$$\vec{X}_{II} = [M_{w,1}, ..., M_{w,8}]^T \tag{20}$$

Due to the substantial heterogeneity of these groups, two separate networks are adopted for the problem of deterioration detection:

- *ANN-I* for detecting material ageing and slackening;
- *ANN-II* for membrane damage detection.

A similar approach was successfully implemented by Hansen and Salamon (1990), where neural network ensembles were used for dealing with large and complex problems. In comparison to a single ANN with a lot of inputs and large weight matrices, particular networks are much easy to be developed and trained to provide good results for a small cost.

Considering, that $\vec{X}$ and $\vec{Y}$ vectors are of the same length and adopting three symmetrical hidden layers (h = 3), the general ANN's structure becomes the following $N_0 - N_1 - N_2 - N_1 - N_0$ (Fig. 9).

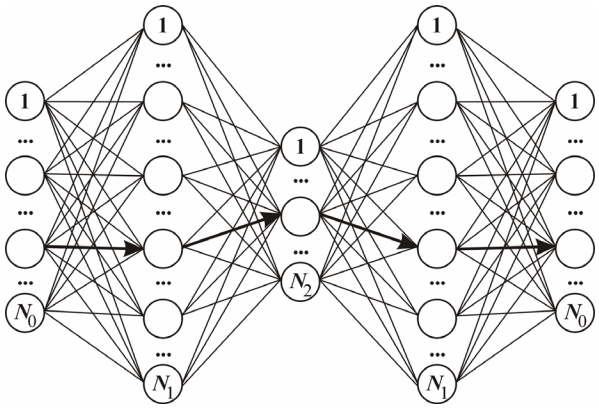

Fig. 9. General structure of the ANN

The size of the first hidden layer of the ANNs adopted is three times as large as the input layer $N_1 = 3 \cdot N_0$. The remaining hyperparameter to be defined is the middle layer size N_2. It allows to investigate so-called "bottle-neck" shape of the ANN, which is intended for extracting hidden features and reducing the noise in the input data (Luo & Nagarajan, 2018).

4. Results and discussion

4.1. Artificial neural networks implementation

The artificial neural networks *ANN-I* and *ANN-II* are implemented using general-purpose computational software MathCad. The graphs of misclassified cases given the number of neurons in the middle layer N_2 are in Figure 10.

In the case of detection of material ageing and slackening (Fig. 10a), the growth of the middle layer

size results in fast attenuation of the false-negative rate and steady increase of the false-positive rate. It can be explained by the over-fitting of the *ANN-I*, which provides smaller discrepancies δ_{max} (4) for the training samples, resulting in less threshold values Δ_{max} (5). So, three neurons ($N_2 = 3$) are adopted for the middle layer of the *ANN-I*, because further increase results in diminishing of quality of the classification.

The network *ANN-II* in case of an insufficient number of neurons (e.g., $N_2 = 1$ or $N_2 = 3$, Fig. 10b) can not store all the data provided. It results in high discrepancies δ_{max} (4) both for the testing and the operational datasets. The network's capacity increases with the growth of the middle layer size. The problem of over-fitting, however, arises for the large network. Seven neurons ($N_2 = 7$) are adopted for the *ANN-II*, because further growth of the middle layer results in negligible diminishing of the false-negative rate. The false-positive rate, however, and especially the computational time for training the network increase substantially.

Thus, the final structures of the networks *ANN-I* and *ANN-II* are the following: 3 – 9 – 3 – 9 – 3 and 8 – 24 – 7 – 24 – 8. The discrepancies δ_{max} (4) for the training datasets are shown in Figure 11.

The threshold needed to separate normal and deteriorated constructions using *ANN-I* is $\Delta_{max,I} = 0.076$, while for *ANN-II* it is $\Delta_{max,II} = 0.029$ (Fig. 11). The data-points are considered normal below these values, while the regions above the thresholds are anomalous. An examined construction with anomalous parameters is considered deteriorated.

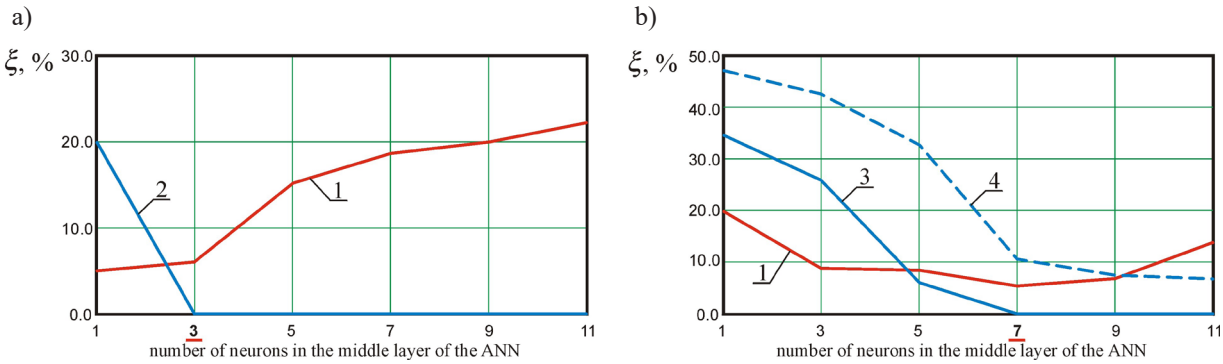

Fig. 10. Graphs of misclassified cases versus the number of neurons in the middle layer N_2: a) *ANN-I*; b) *ANN-II*; 1 – false-positive rate (6), ξ_p; 2–4 – false-negative rates (7), ξ_n; 2 – polymer membrane slackening case on a quarter of the surface; 3 – membrane tearing case in sector 1; 4 – membrane tearing case in sector 4

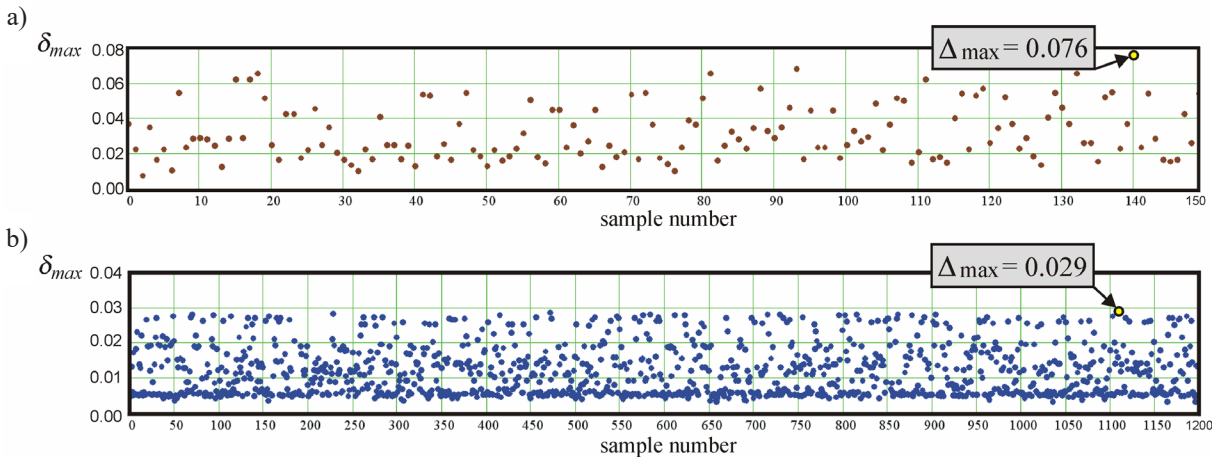

Fig. 11. Discrepancies δ_{max}, obtained for the trained networks using the training samples: a) network *ANN-I*; b) network *ANN-II*

4.2. Detection of material deterioration

The discrepancies (4) obtained for testing (normal) $\vec{\Omega}_{test}$ and operational (deteriorated) $\vec{\Omega}_{op}$ datasets are shown in figures 12 and 13.

According to condition (3), the networks provide results for reliable classification of not deteriorated constructions into the normal class. The misclassification (false positive rate ξ_p) is 6.7% for the *ANN-I* and 5.4% for the *ANN-II* (Figs. 12a and 13a).

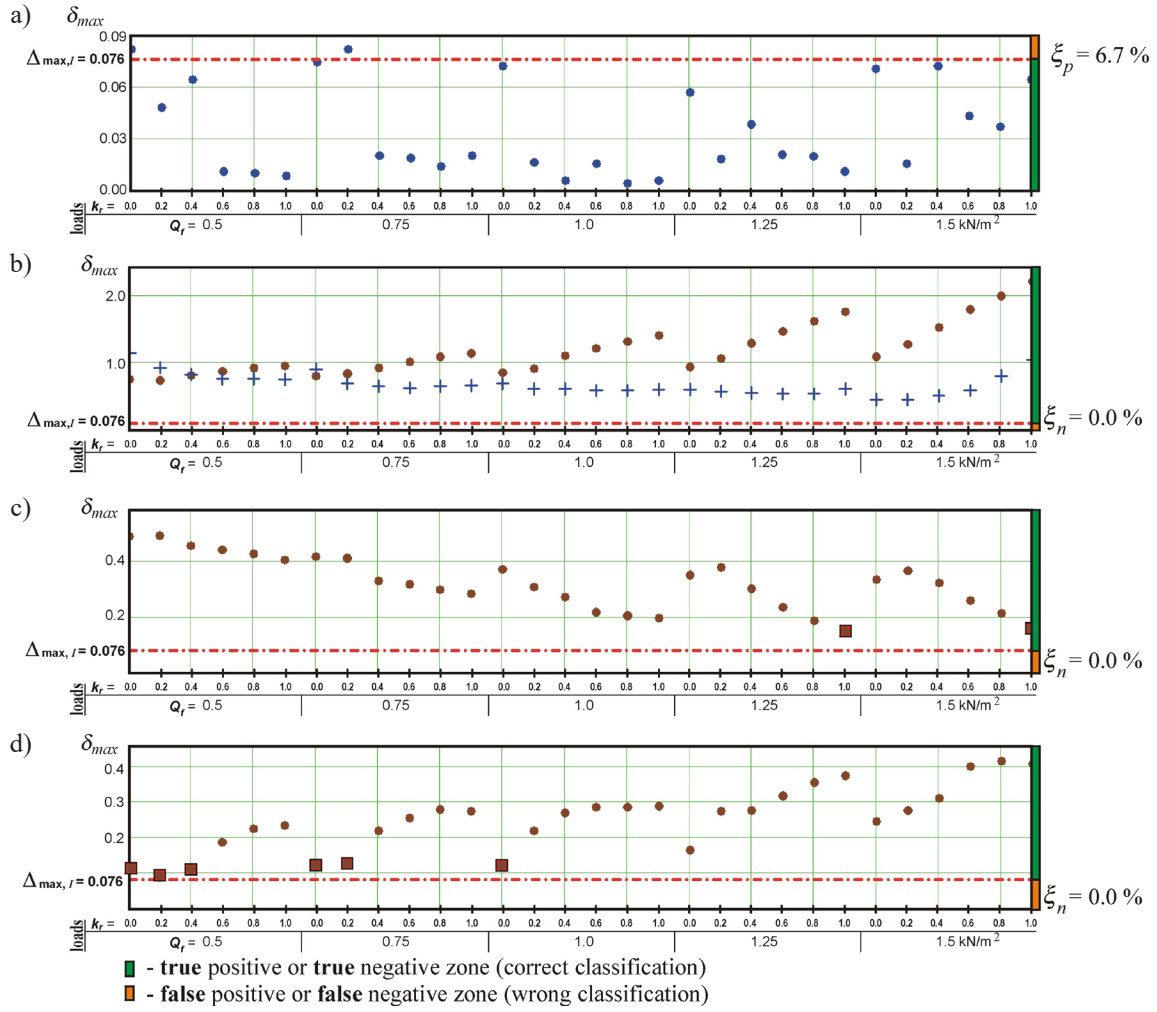

Fig. 12. Discrepancies (4) obtained using the trained network *ANN-I*: a) δ_{max}-values for the testing samples (no material deterioration); b)–d) δ_{max}-values for the operational samples: b) fiberglass top chord ageing (all the elements and a single one); c), d) polymer membrane slackening on the whole surface and on a quarter of the surface, respectively

The top chord ageing, as well as catenary cables and membrane slackening, are uniquely detected using the condition (3) applied for the results provided by the *ANN-I*: the misclassification (false negative rate ξ_n) is zero for all the listed types of the deterioration (Figs. 12b–12d).

Fiberglass top chord ageing is reliably detected due to large values of the discrepancies δ_{max}, which far exceed the threshold $\Delta_{max,I}$. The discrepancies δ_{max} obtained for membrane and cable slackening are very close to each other and can't be visually distinguished (graphs for polymer membrane slackening are only indicated in Figures 12c and 12d).

In the case of slackening of the whole surface (Fig. 12c), uniformly distributed external loads (reduction coefficient $k_r \rightarrow 1.0$) decrease the classification reliability because the discrepancies δ_{max} (denoted by square signs) tend to the threshold. Non-uniformly distributed external loads ($k_r \rightarrow 0.0$), in turn, may potentially cause a misclassification error in cases of cable or membrane slackening on a quarter of the surface (Fig. 12d).

Membrane tearing situated in the first sector of the surface (sector numbers in the local coordinate system (X_{loc}, Y_{loc}, Z) are in Figure 3) is detected correctly using the *ANN-II*. The damage prediction reliability increases in accordance with the growth of external load value Q_f and decreases with the growth of external load uniformity ($k_r \rightarrow 1.0$) (Fig. 13b).

The remaining sectors shifted from the fully loaded area of the membrane to the reduced load zone, are harder to be classified into damaged and normal types. The false-negative rate ξ_n is 0.4%, 3.3% and 10.4% for the sectors 2–4, respectively (Figs. 13c–13e).

The samples misclassified using *ANN-II* belong to non-uniformly distributed external loads ($k_r \rightarrow 0.0$). The growth of the classification error indicates that a low level of external load poorly influences the reliability of the damage detection.

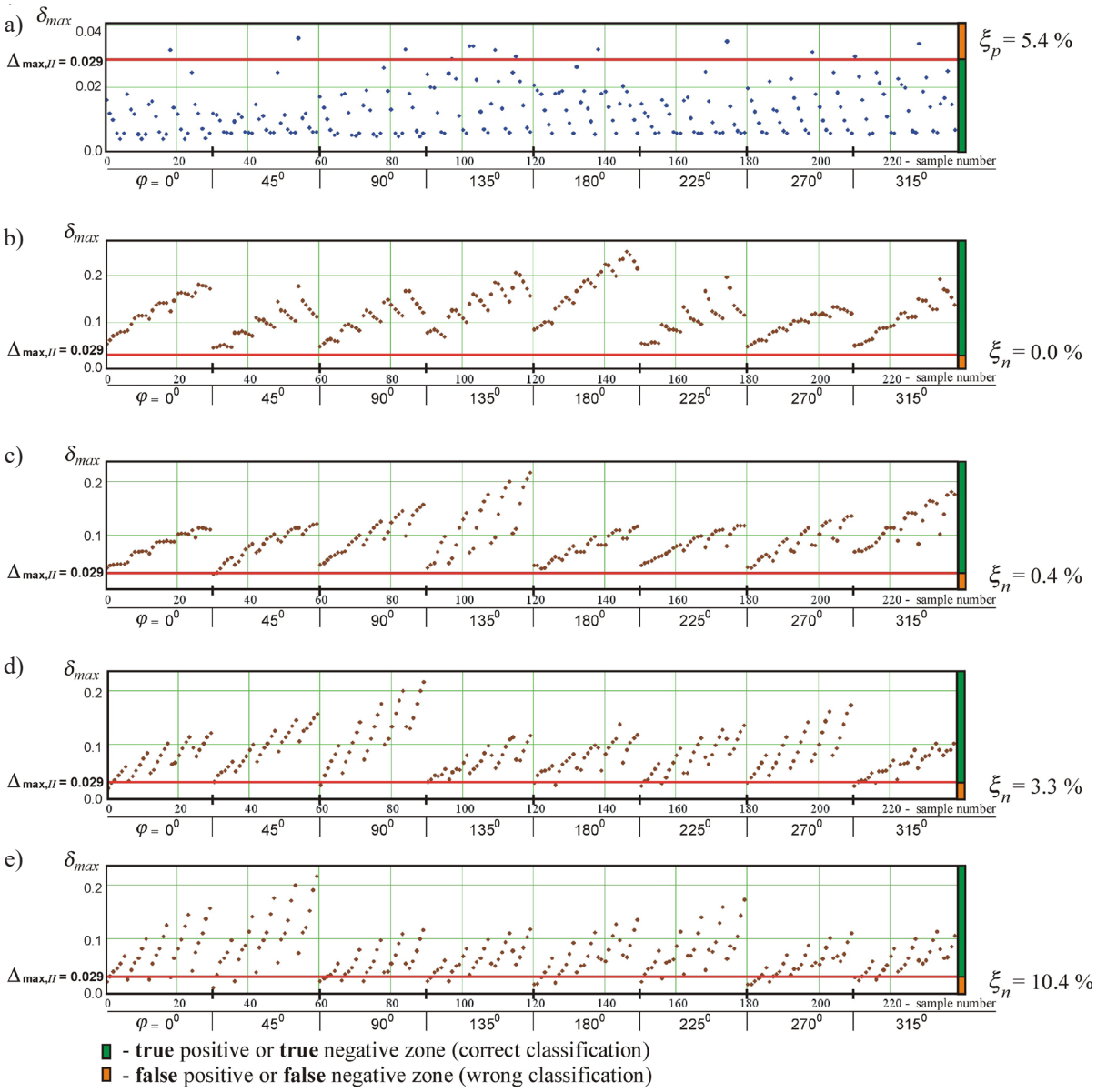

Fig. 13. Discrepancies (4) obtained using the trained network *ANN-II*: a) δ_{max}-values for the testing samples (no material deterioration); b)–e) δ_{max}-values for the operational samples (tearing in sectors 1–4 of the membrane, respectively, Fig. 3d)

5. Conclusions

1. The problem of detection of material deterioration in hybrid building constructions is considered. Artificial Neural Networks (ANNs) and semi-supervised learning approaches are used. The approach is in the classification of the construction into normal and anomalous (deteriorated) classes judging by the discrepancy between a given vector of structural parameters (features) and the resultant vector generated by the trained ANN.
2. Training the network and obtaining the classification threshold only need normal data which are collected from the construction without any defects or deterioration.
3. False-positive and false-negative error metrics are used to assess the quality of the classification.
4. Appropriate ANN structures and required features are proposed for two different types of deterioration cases: material ageing and slackening (network *ANN-I*), as well as membrane tearing (network *ANN-II*). The sizes of the middle layers of both ANNs are adopted using the error metrics considered.

   Both the networks provide results for the reliable classification of not deteriorated constructions into

the normal class. The misclassification (false positive rate ξ_p) does not exceed 6.7%.

The top chord ageing, as well as catenary cables and membrane slackening, are uniquely detected using the *ANN-I*. The misclassification (false-negative rate ξ_n) is zero for all the types of deterioration.

Membrane damages (the local slits) are detected correctly in most cases using the *ANN-II*. The misclassification depends on the slit location relatively to the position of non-uniform external load. Transitioning the slit from the fully loaded to not loaded area of the membrane results in the following growing trend of the false-negative rate ξ_n: 0.0%, 0.4%, 3.3%, and 10.4%. Considering that the misclassified cases correspond to a low level of external load, they are much less influential on the survivability of the construction than correctly detected slits in the fully loaded membrane sectors.

5. The work contributes to the structural health monitoring of hybrid building constructions. It provides a possibility to detect material deterioration given the forces in particular structural elements. The next step of the research is the transition from numerically obtained forces to real gauging equipment indications collected in real-time from a real construction. The problems of noise in the sensors' data and the optimum arrangement of the gauging devices remain to be tackled and should be considered of primary importance.

References

Bridgens, B.N., Gosling, P.D., & Birchall, M.J.S. (2004). Tensile fabric structures: concepts, practice and developments. *The Structural Engineer*, *82*(14), 21–27.

Chandola, V., Banerjee, A., & Kumar, V. (2009). Anomaly detection: a survey. *ACM Computing Surveys*, *41*(3), article 15, 1–58. https://doi.org/10.1145/1541880.1541882.

Chesnokov, A.V., Mikhailov, V.V., & Dolmatov, I.V. (2017). Bending-active dome-shaped structure. In K. Bletzinger, E. Oñate, & B. Kröplin (Eds.). *VIII International Conference on Textile Composites and Inflatable Structures*. *Structural membranes 2017. 9–11 october 2017, Munich, Germany* (pp. 427–435). http://congress.cimne.com/membranes2017/frontal/Doc/Ebook2017.pdf.

Chesnokov, A.V., Mikhailov, V.V., & Dolmatov, I.V. (2019). Bending-active frame: analysis and estimation of structural parameters. In A. Zanelli, C. Monticelli, M. Mollaert, B. Stimpfle (Eds.). *Proceedings of the TensiNet Symposium. Softening the habitats. Sustainable innovation in minimal mass structures and lightweight architectures* (pp. 111–122).

Colasante, G., & Gosling, P.D. (2016). Including shear in a neural network constitutive model for architectural textiles. In J. Chilton, P. Gosling, M. Mollaert, & B. Stimpfle (Eds.). *TENSINET – COST TU1303 International Symposium 2016 "Novel structural skins – Improving sustainability and efficiency through new structural textile materials and designs"* (pp. 103–112). "Procedia Engineering", vol. 155. https://www.sciencedirect.com/journal/procedia-engineering/vol/155/suppl/C.

Gipperich, K., Canobbio, R., Lombardi, S., & Malinowsky, M. (2004). Fabrication, installation and maintenance. In B. Forster, & M. Mollaert (Eds.). *European Design Guide for Tensile Surface Structures* (pp. 243–254). TensiNet.

Hansen, L.K., & Salamon, P. (1990). Neural network ensembles, *IEEE Transactions on Pattern Analysis and Machine Intelligence*, *12*(10), 993–1001. https://doi.org/10.1109/34.58871.

Hodge, V.J., & Austin, J. (2004). A survey of outlier detection methodologies. *Artificial Intelligence Review*, *22*(2), 85–126.

Horr, A.M., Asadsajadi, S.R., & Safi, M. (2003). Design of large space structures with imperfection using ANN-based simulator. *International Journal of Space Structures*, *18*(4), 235–255. https://doi.org/10.1260/026635103322987968.

Kaveh, A., & Dehkordi, M.R. (2003). Neural networks for the analysis and design of domes, *International Journal of Space Structures*, *18*(3), 181–193. https://doi.org/10.1260/026635103322437463.

Lienhard, J., Alpermann, H., Gengnagel, C., & Knippers, J. (2013). Active bending, a review on structures where bending is used as a self-formation process, *International Journal of Space Structures*, *28*(3–4), 187–196. https://doi.org/10.1260/0266-3511.28.3-4.187.

Luo, T., & Nagarajan, S.G. (2018). Distributed anomaly detection using autoencoder neural networks in WSN for IoT. In *2018 IEEE International Conference on Communications (ICC)* (pp. 1–6). https://doi.org/10.1109/ICC.2018.8422402.

Osovskiy, S. (2002). *Neyronnyye seti dlya obrabotki informatsii*. Finansy i statistika [Осовский, С. (2002). *Нейронные сети для обработки информации*. Финансы и статистика].

Pozo, F., Tibaduiza, D.A., Anaya, M., & Vitola, J. (2017). A machine learning methodology for structural damage classification in structural health monitoring. In A. Guemes, A. Benjeddou, J. Rodellar, & J. Leng (Eds.). *8th ECCOMAS Thematic Conference on Smart Structures and Materials. SMART 2017* (pp. 698–708). http://congress.cimne.com/smart2017/frontal/Objectives.asp.

Sommerville, J. (2007). Defects and rework in new build: an analysis of the phenomenon and drivers. *Structural Survey*, *25*(5), 391–407. https://doi.org/10.1108/02630800710838437.

Thimm, G., & Fiesler, E. (1995). Neural network initialization. In J. Mira, F. Sandoval (Eds.). *From Natural to Artificial Neural Computation* (pp. 533–542), IWANN.

Van Mele, T., De Laet, L., Veenendaal, D., Mollaert, M., & Block, P. (2013). Shaping tension structures with actively bent linear elements, *International Journal of Space Structures*, *28*(3–4), 127–135. https://doi.org/10.1260/0266-3511.28.3-4.127.

Wang, C., Abdul-Rahman, H., Wood, L.C., Mohd-Rahim, F.A., Zainon, N., & Saputri, E. (2015). Defects of tensioned membrane structures (TMS) in the Tropics. *Journal of Performance of Constructed Facilities*, *29*(2). https://doi.org/10.1061/(ASCE)CF.1943-5509.0000530.